Supplementary Information (SI) for Energy & Environmental Science.
This journal is © The Royal Society of Chemistry 2024

Electronic Supplementary Information

Defect-enabled local high temperature field within carbon to promote in-plane integration of electrocatalyst for CO_2-to-CO conversion

Yafang Zhang,[1] Chang Yu,[1,*] Xuedan Song,[1] Xinyi Tan,[1] Wenbin Li,[1] Shuo Liu,[1] Xiuqing Zhu,[1] Song Cui,[1] Yuanyang Xie,[1] Jieshan Qiu[2,*]

[1] State Key Laboratory of Fine Chemicals, Liaoning Key Lab for Energy Materials and Chemical Engineering, School of Chemical Engineering, Dalian University of Technology, Dalian, 116024, China.
[2] State Key Laboratory of Chemical Resource Engineering, College of Chemical Engineering, Beijing University of Chemical Technology, Beijing, 100029, China.

*Corresponding author.

E-mail: chang.yu@dlut.edu.cn, qiujs@mail.buct.edu.cn

Methods

Chemicals

The raw materials involve multi-walled carbon nanotube (MWCNT, abbreviated as CNT), N, N-dimethylformamide (DMF), Hemin, N-methylpyrrolidone (NMP), pyrrole, ammonium persulfate [$(NH_4)_2S_2O_8$; APS], thionyl chloride ($SOCl_2$), 4-dimethylaminopyridine (DMAP), triethylamine, urea, iron phthalocyanine (FePc), iron nitrate ($Fe(NO_3)_3$), cobalt phthalocyanine (CoPc), and nickel phthalocyanine (NiPc).

Synthesis of H/DCNT and DCNT

The H/DCNT was prepared in a specially-modified domestic microwave oven. Specifically, 100 mg CNT and 2 mg Hemin were dispersed in 5 mL DMF within a home-made quartz tube. Then the quartz tube was placed in a sonicated device and treated for 30 minutes. Next, the mixture together with the quartz tube were transferred into microwave oven and introduced continuous nitrogen flow (15 sccm) to remove air. Further, the tube was exposed under microwave irradiation for 10 minutes, where the nitrogen flow was still kept to purge the gasified/pyrolyzed DMF. Finally, the solid phase was collected and ground into powder, which was noted as H/DCNT. Additionally, the DCNT was also prepared following the above method, where the only difference was without Hemin as precursor.

Synthesis of L-H-CNT and π-H-CNT

The L-H-CNT and π-H-CNT samples were prepared following the previously reported method.[1] For L-H-CNT, two procedures, aminated process and chemical grafting, were included. Specifically, for aminated CNT, 9.0 g of CNT was first mixed with 50 mL of NMP and sonicated for 2 hours. The CNT suspension was further mixed with pyrrole solution (400 μL pyrrole/100 mL deionized water) and kept at 4 °C for 1 hour. Under constant stirring, 50 mL of 0.06 M APS aqueous solution was added dropwise. The mixture was then stirred continuously at 4 °C for 24 hours. After washing by filtration and drying at 80 °C for 6 hours, the aminated CNT is obtained. Additionally, for L-H-CNT, 126 mg of Hemin and 43.2 μL of $SOCl_2$ were dissolved in 10 mL of DMF, sonicated for 10 min and then 72.9 mg of DMAP was added. Next, 120 mg of aminated CNT was dispersed in 30 mL of DMF, 208 μL of triethylamine was added and the mixture was sonicated for 45 min. Further, the former was added dropwise to the latter under constant stirring and the resulting mixture was kept at 80 °C for 24 h. The product was filtered, washed and dried at 60 °C for 12 hours and L-H-CNT was obtained.

For π-H-CNT, 100 mg CNT and 2 mg Hemin were dispersed in 5 mL DMF and further stirred continuously under room temperature (RT) for 12 hours. Then the mixture was filtered, washed and dried at 80 °C for 12 hours to prepare the π-H-CNT.

Synthesis of h-H/CNT, u-H/CNT and w-H/CNT

For h-H/CNT, the synthetic method was similar to that of H/DCNT but 5 mL DMF was changed to 5 mL H_2O. For u-H/CNT, 100 mg CNT, 2 mg Hemin and 1.947 g urea were mixed and filled into the home-made quartz tube. After purging for 30 min in continuous yet flowing nitrogen (15 sccm), the mixture was irradiated by microwave for 10 minutes, and the nitrogen flow was kept during all the process. For w-H/CNT, the method is the same as that of u-H/CNT, without urea.

Synthesis of FePc/DCNT, CoPc/DCNT, NiPc/DCNT, and $Fe(NO_3)_3$/DCNT

The FePc/DCNT, CoPc/DCNT, NiPc/DCNT, and $Fe(NO_3)_3$/DCNT were prepared, where 2 mg Hemin was replaced by FePc, CoPc, NiPc, and $Fe(NO_3)_3$ of equal quality, respectively.

Characterization

The morphology was observed by HR-TEM (JEM-F200, JEOL) and HAADF-STEM (Titan, FEI). The crystalline structure was analyzed by XRD equipped with Cu Kα radiation (D/MAX-2400, Rigaku). The vibration and structure information of the molecules were acquired by FTIR (INVENIO-R, Thermo) and Raman (Fisher Scientific DXR, Thermo) spectra. The surface composition and electronic state information were detected by XPS (ESCALAB250, Thermo). XAFS (4B9A beamline, Beijing Synchrotron Radiation Facility) was used to decouple the coordination environment and fine structure. The iron element contents were detected by ICP-OES (Optima2000DV, PerkinElmer). At room temperature, the structure vacancies were obtained through EPR spectra (E500, Bruker), where the measurement frequency was 9.42 GHz. The contact potential difference was revealed by KPFM (Dimension Icon, Bruker), and highly oriented pyrolytic graphite (HOPG) was used as substrate in the test. The dielectric properties were obtained from vector network analyzer (PNA-N5244A, Agilent) at a detection range of 1-18 GHz, where the samples were added into paraffin (mass ratio of 10 wt%) and further squeezed into toroidal shape (inner diameter, outer diameter and thickness were 3.04, 7, and 2 mm, respectively).

Electrochemical measurements

For the electrochemical measurements in H-type cell and flow cell, the data was collected and recorded by the CHI 1140E electrochemical workstation (Shanghai ChenHua Instrument Corporation, China) and the Corrtest CS310M electrochemical workstation (Wuhan Corrtest Instrument, China). The as-mentioned potentials were all corrected against the reversible hydrogen electrode (RHE). The potentials were all recorded with 100% *iR* compensation (equation 1).

$$E_{\mathrm{RHE}} = E_{\mathrm{Ag/AgCl}} + 0.0591 \times \mathrm{pH} + 0.210 - iR \tag{1}$$

Specifically, 4 mg catalyst was dispersed in ethanol (970 μL) and 5 wt% Nafion solution (30 μL) to make ink. In the typical three-electrode system, the catalyst was loaded on the working electrode, Ag/AgCl electrode served as the reference electrode, the Pt sheet and Ni foam were selected as counter electrode in H-type cell and flow cell, respectively. Nafion 117 film was used as a proton exchange membrane to separate the compartment of the cathode and anode.

For H-type cell, 50 μL ink was sprayed onto the surface of a 12 mm glassy carbon electrode. The electrolyte was 0.1 M CO_2-saturated $KHCO_3$ and CO_2 was continuingly pumped with a flow rate of 30 sccm. For flow cell, the catalyst ink was pipetted onto the gas diffusion layer (GDL, Sigracet 22BB, effective area of 0.5*2 cm^2), which was further dried at 60 °C, repeating the circle until the loaded quality of the catalyst reached 0.5 mg cm^{-2}. Moreover, the cathode electrolyte was 1 M $KHCO_3$ with a pump rate of 5 sccm, and CO_2 was supplied to the backside of GDL with a flow rate of 15 sccm.

For the electrochemical measurements in MEA electrolyzer, the electrochemical signal was provided and recorded by a DC power supply (WYG-30V200A), without *i*R correction. The preparation of the cathode electrode was similar to that in the flow cell, the catalyst ink was pipetted onto the GDL (Sigracet 38BC), with an effective area of 5*5 cm^2. The anode electrode was a Ti felt loaded with IrO_2 and an anion exchange membrane (Sustainion X37-50-grade 60) was placed between cathode and anode. The loading mass of the catalysts were 1 mg cm^{-2} at cathode (H/DCNT) and 4 mg cm^{-2} at anode (IrO_2), respectively. Additionally, 1 M $KHCO_3$ was pumped to anode with a rate of 50 sccm and there was no electrolyte in cathode, while humid CO_2 was transported with a rate of 180 sccm.

CO_2RR product analysis

The gas products for the electrochemical reduction of CO_2 were delivered into a gas chromatograph (GC7900, Techcomp) to complete the quantitive/qualitative identification. Liquid products are quantified by analyzing the collected electrolytes using NMR (AVANCE NEO 600M, Bruker). The Faradaic efficiency (*FE*) for electrochemical CO_2 conversion was calculated as equation 2:

$$FE = \frac{\alpha \mathrm{F} P}{i} \times \frac{v \times 10^{-6} \times u_{\mathrm{CO_2}}}{\mathrm{R}T} \tag{2}$$

where α is the number of transferred electrons when one molecular product is produced (here is 2), F indicates the Faradaic constant (96485 C $\mathrm{mol^{-1}}$), P is the room pressure (101325 Pa), i is the test current, v is the ratio of the reduction product, $u_{\mathrm{CO_2}}$ is the flow rate of CO_2, R is the gas constant (8.314 J $\mathrm{mol^{-1}}$ $\mathrm{K^{-1}}$) and T is the room temperature (298 K).

The turnover frequency (TOF) was calculated by equation 3:

$$\mathrm{TOF} = \frac{i_{\mathrm{CO}} / \alpha \mathrm{F}}{\omega \times m_{\mathrm{catalyst}} / \mathrm{M_{Fe}}} \times 3600 \tag{3}$$

where i_{CO} is the partial current for CO, ω is the mass ratio of Fe atoms in the catalysts, which is confirmed through the inductively coupled plasma optical emission spectroscopy with a value of 0.24 wt%, m_{catalyst} is the mass in the electrode (which is $2*10^{-4}$ g in the H-type cell and $5*10^{-4}$ g in the flow cell), and $\mathrm{M_{metal}}$ is the atomic mass of Fe.

The Energy efficiency (*EE*) for the flow cell was evaluated as equation 4 (for flow cell) and equation 5 (for MEA):

$$EE = \frac{1.23 - E_0}{1.23 - E} \times FE \tag{4}$$

$$EE = \frac{1.23 - E_0}{E_{\mathrm{Cell}}} \times FE \tag{5}$$

where E_0 is the standard potential (−0.11 V vs. RHE for CO_2-to-CO conversion) and E in equation 4 is the applied potential. E_{Cell} is the total cell voltage obtained from the MEA experiment in equation 5.

CO yield can be obtained from equation 6:

$$\text{CO yield} = \frac{j_{\mathrm{CO}}}{\alpha \mathrm{F}} \times 3600 \tag{6}$$

where α is 2 and F is 96485 C $\mathrm{mol^{-1}}$.

CO_2 conversion efficiency was deduced on the basis of CO yield, as equation 7:

$$CO_2 \text{ conversion efficiency} = \frac{\text{CO yield} \times S}{u_{\mathrm{CO_2}}} \tag{7}$$

where S indicates the effective area of GDL (0.5*2 $\mathrm{cm^2}$) and the value of $u_{\mathrm{CO_2}}$ is 15 sccm.

Finite element analysis (FEA)

COMSOL Multiphysics was used to perform the computational model and analysis the dissipated microwave power distribution. The model of the microwave oven was a coppery metallic box, where the box was filled with nitrogen and a 2.45 GHz microwave source was provided via a rectangular waveguide. The waveguide was placed at the bottom of the metallic box and was much larger than the inner object model, referring to the actual situation. A hollow cylinder was placed in the middle of the box to serve as the geometry model of CNT support, with a length of 180 nm and the diameter of 30 nm. Moreover, five evenly arranged round holes were added on the surface of the hollow cylinder to act as the geometry model of the defective CNT (DCNT), while the diameter of these holes was 4 nm.

DFT calculation

Vienna ab initio simulation package (VASP) [2] was used to carry out the spin-polarized DFT calculations[3, 4]. Pseudopotentials established by the projector-augmented wave (PAW) method and the Perdew−Burke−Ernzerh (PBE)[5] exchange-correlation functional, within the Van der Waals (vdW) correction developed by Grimme (DFT + D3).[6] The cut-off energies for plane waves were set to 500 eV. The energy in the iterative process was less than 10^{-4} eV, and the threshold for force was 0.05 eV $Å^{-1}$. For all calculations, a 3 × 3 × 1 Monkhorst–Pack k-mesh was adopted. The implicit solvent model implemented by VASPsol was used, with a dielectric constant of 80.[7]

Adsorption energy (E_{ad}) was calculated using the equation: $E_{\mathrm{ad}} = E_{\mathrm{total}} - E_{\mathrm{substrate}} - E_{\mathrm{adsorbate}}$, where E_{total}, $E_{\mathrm{substrate}}$, and $E_{\mathrm{adsorbate}}$ are the energies of the total system, the substrate, and the adsorbate, respectively. Gibbs free energy change (ΔG) was calculated according to the equation: $\Delta G = \Delta E_{\mathrm{DFT}} + \Delta E_{\mathrm{ZPE}} - T\Delta S + \Delta G_{\mathrm{pH}} + \Delta G_{\mathrm{U}}$. Among which, ΔE_{DFT}, ΔE_{ZPE} and ΔS refer to the changes of the electronic energy derived from the DFT calculation, the zero-point energy and the entropy, respectively. Moreover, $\Delta G_{\mathrm{pH}} = \mathrm{pH} \times k_{\mathrm{B}}T \ln 10$ and $\Delta G_{\mathrm{U}} = -neU$, where pH is regarded as 0, k_{B}, n, and U denote to Boltzmann constant, the transferred electron number, and the electrode potential, respectively. Additionally, T represents the reaction temperature of 298.15 K.

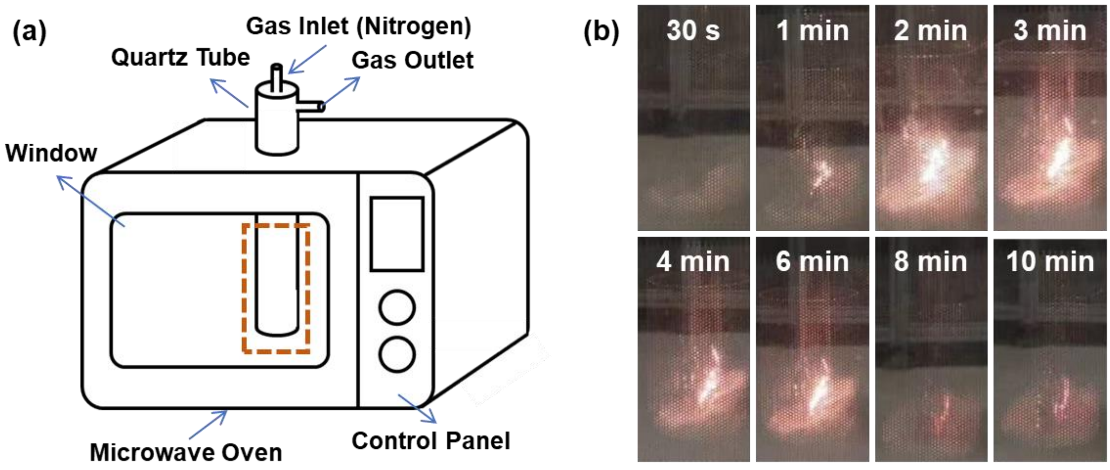

Figure S1. (a) The schematic diagram for the structure of the microwave reactor. (b) The photographs of the reaction process within 10 minutes, and the region is the dotted box established in Fig S1a.

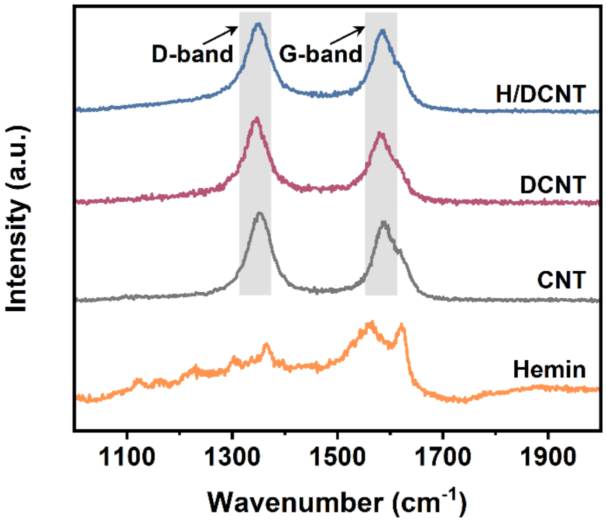

Figure S2. Raman spectra of H/DCNT, DCNT, CNT and Hemin samples.

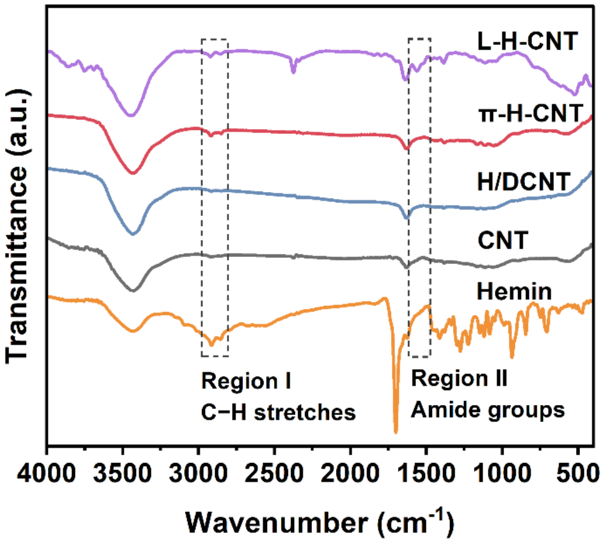

Figure S3. FTIR spectra of L-H-CNT, π-H-CNT, H/DCNT, CNT, and Hemin.

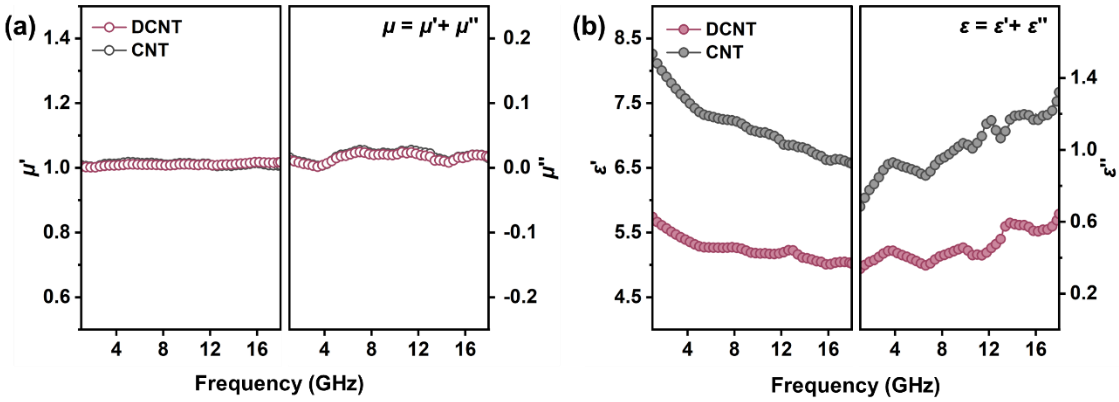

Figure S4. (a) Complex relative permeability and (b) complex relative permittivity of CNT and DCNT samples.

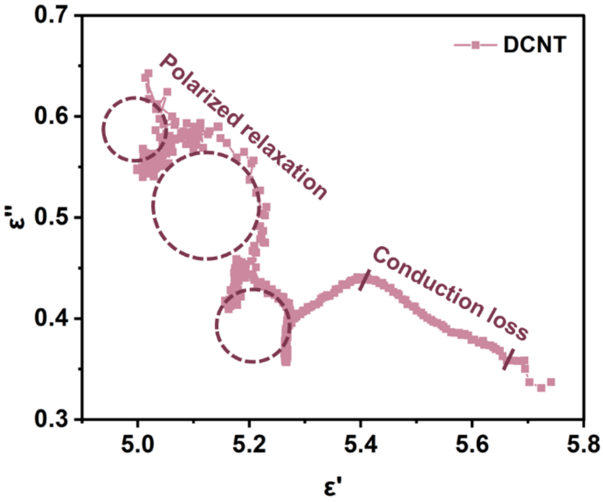

Figure S5. Cole-Cole plot of DCNT sample.

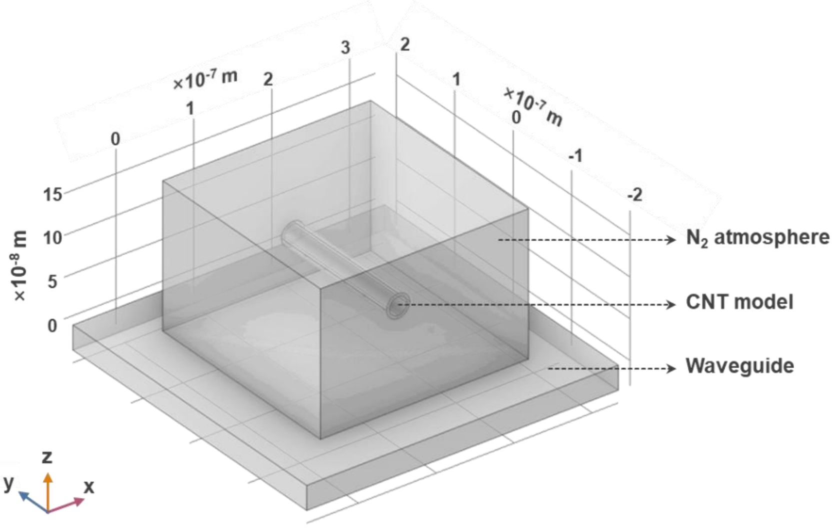

Figure S6. The geometric model of COMSOL simulation, where the CNT models with/without surface defects were established and placed under the microwave condition.

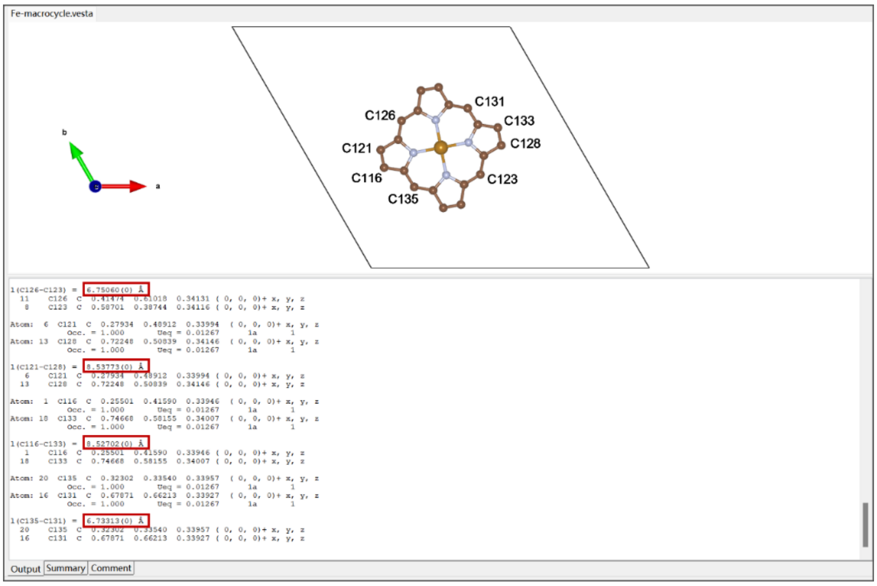

```
l(C126-C123) =  6.75060(0) Å
  11    C126  C  0.41474  0.61018  0.34131 ( 0, 0, 0)+ x, y, z
   8    C123  C  0.58701  0.38744  0.34116 ( 0, 0, 0)+ x, y, z

Atom:  6  C121  C  0.27934  0.48912  0.33994  ( 0, 0, 0)+ x, y, z
          Occ. = 1.000       Ueq = 0.01267      1a       1
Atom: 13  C128  C  0.72248  0.50839  0.34146  ( 0, 0, 0)+ x, y, z
          Occ. = 1.000       Ueq = 0.01267      1a       1

l(C121-C128) =  8.53773(0) Å
   6    C121  C  0.27934  0.48912  0.33994 ( 0, 0, 0)+ x, y, z
  13    C128  C  0.72248  0.50839  0.34146 ( 0, 0, 0)+ x, y, z

Atom:  1  C116  C  0.25501  0.41590  0.33946  ( 0, 0, 0)+ x, y, z
          Occ. = 1.000       Ueq = 0.01267      1a       1
Atom: 18  C133  C  0.74668  0.58155  0.34007  ( 0, 0, 0)+ x, y, z
          Occ. = 1.000       Ueq = 0.01267      1a       1

l(C116-C133) =  8.52702(0) Å
   1    C116  C  0.25501  0.41590  0.33946 ( 0, 0, 0)+ x, y, z
  18    C133  C  0.74668  0.58155  0.34007 ( 0, 0, 0)+ x, y, z

Atom: 20  C135  C  0.32302  0.33540  0.33957  ( 0, 0, 0)+ x, y, z
          Occ. = 1.000       Ueq = 0.01267      1a       1
Atom: 16  C131  C  0.67871  0.66213  0.33927  ( 0, 0, 0)+ x, y, z
          Occ. = 1.000       Ueq = 0.01267      1a       1

l(C135-C131) =  6.73313(0) Å
  20    C135  C  0.32302  0.33540  0.33957 ( 0, 0, 0)+ x, y, z
  16    C131  C  0.67871  0.66213  0.33927 ( 0, 0, 0)+ x, y, z
```

Figure S7. The size of Fe-macrocycle that is identified and acquired from the VESTA software.

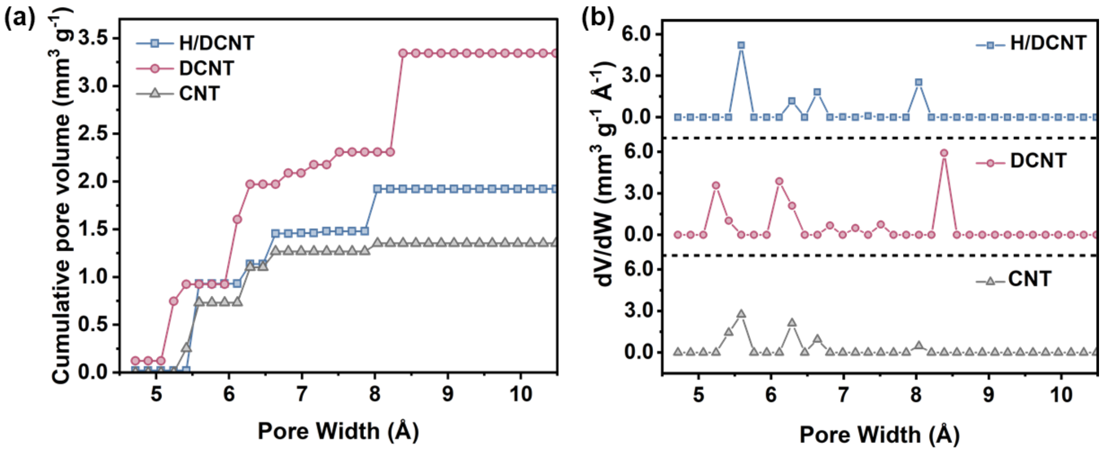

Figure S8. (a) The cumulative pore volume and (b) pore size distribution profiles of H/DCNT, DCNT and CNT.

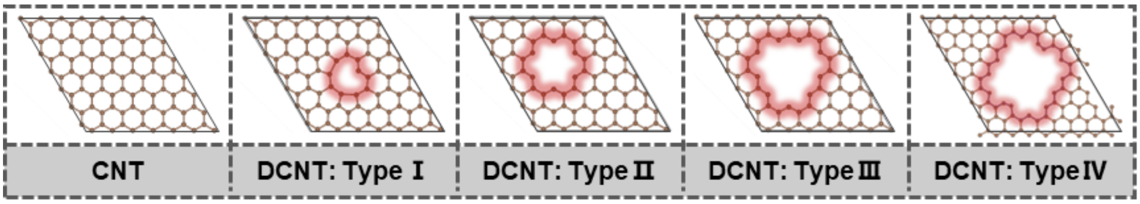

Figure S9. The molecular structure of CNT and DCNT with the different defects.

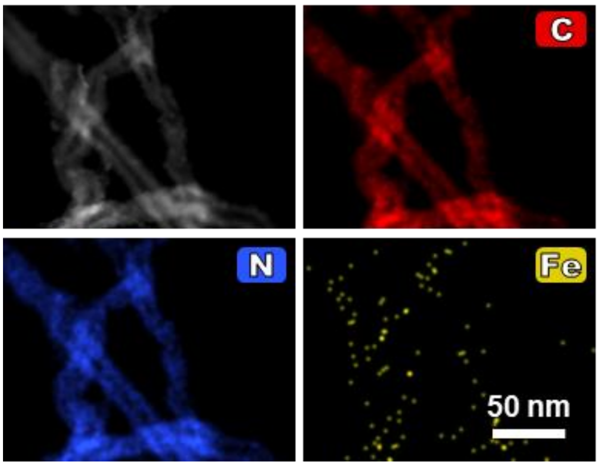

Figure S10. Energy-dispersive X-ray spectroscopy (EDS) mapping images of H/DCNT.

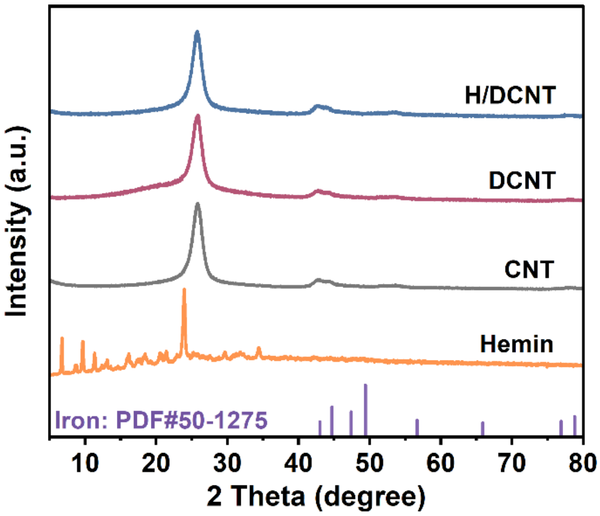

Figure S11. X-ray diffraction (XRD) patterns of H/DCNT, DCNT, CNT and Hemin samples.

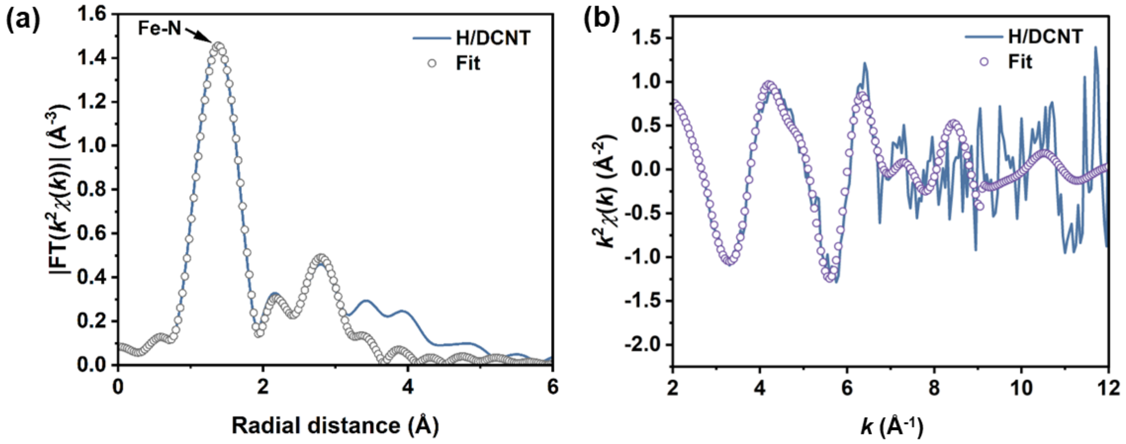

Figure S12. (a) Raw Fourier Transforms (FT) together with the extended X-ray absorption fine structure (EXAFS) fits and (b) the corresponding $k^2\chi(k)$ (Å^{-2}) EXAFS data of H/DCNT.

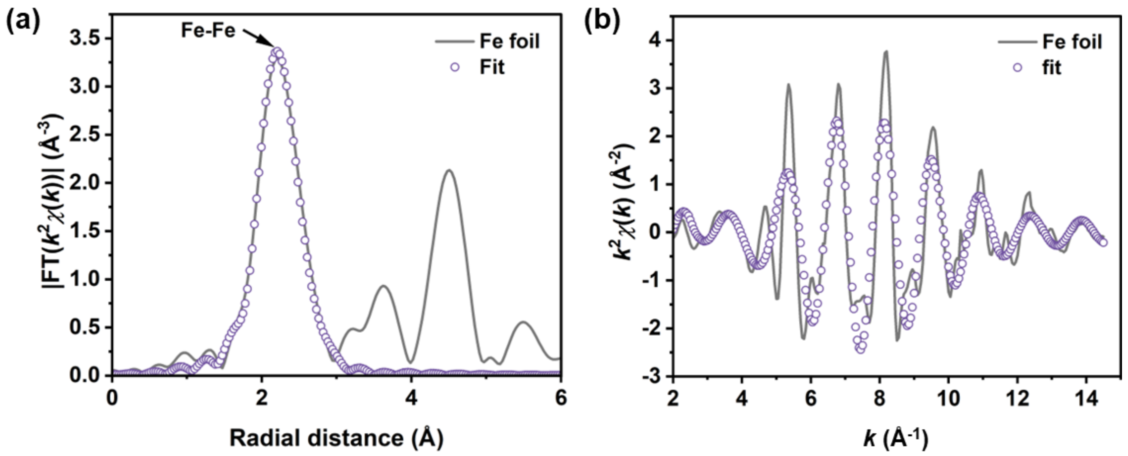

Figure S13. (a) Raw Fourier Transforms (FT) together with the EXAFS fits and (b) the corresponding $k^2\chi(k)$ (Å^{-2}) EXAFS data of Fe foil.

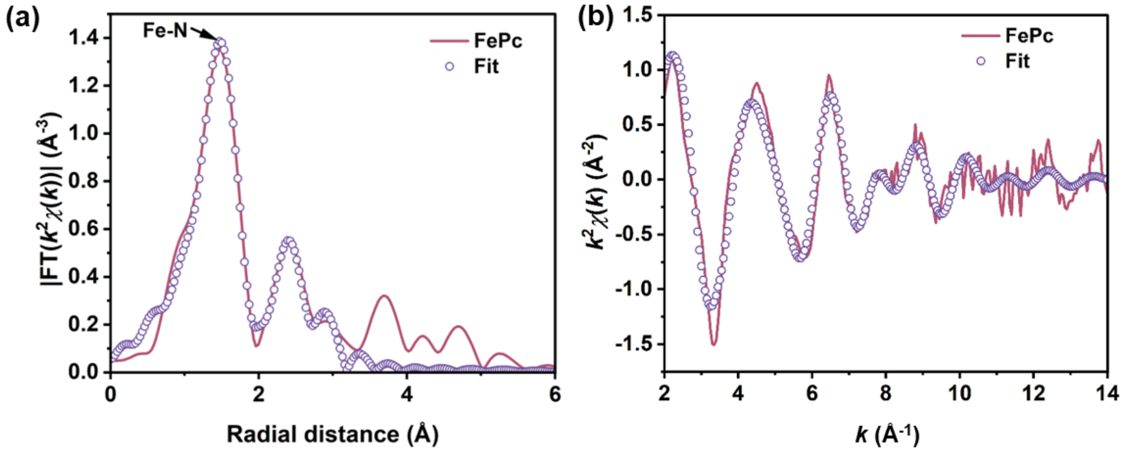

Figure S14. (a) Raw Fourier Transforms (FT) together with the EXAFS fits and (b) the corresponding $k^2\chi(k)$ (Å^{-2}) EXAFS data of FePc.

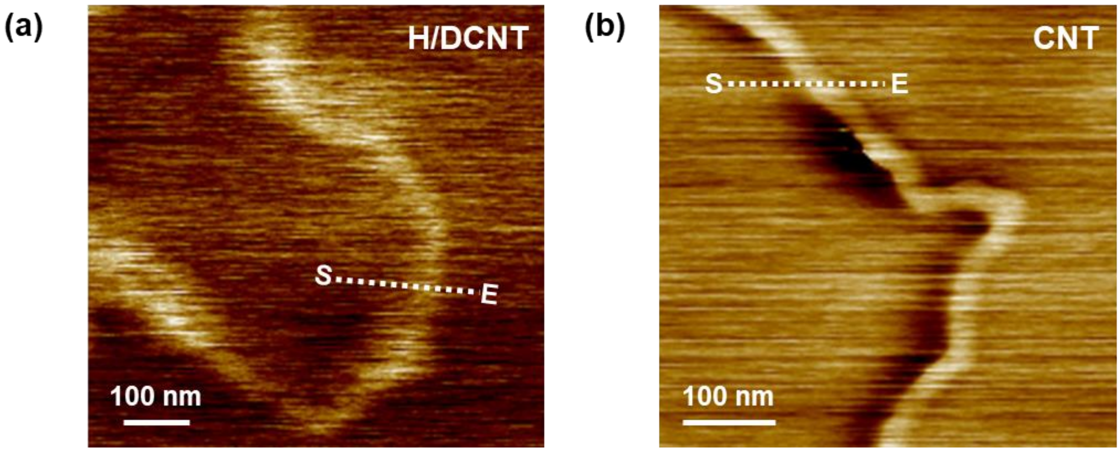

Figure S15. Topography images of (a) H/DCNT and (b) CNT, where the white dotted lines represent the measurement position for contact potential difference (CPD), the letters of “S” and “E” are on behalf of the start point and end point, respectively.

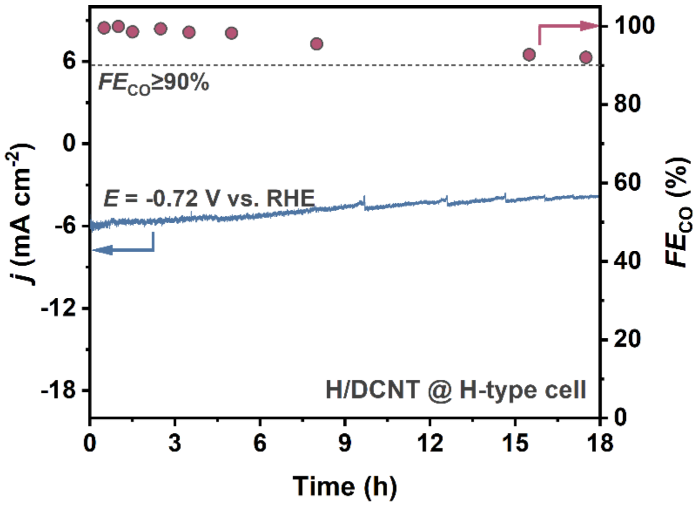

Figure S16. Durability test at −0.72 V vs. RHE in H-type cell.

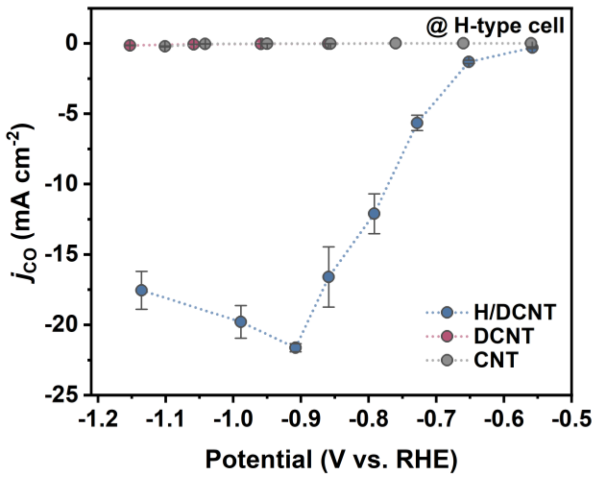

Figure S17. j_{CO} over H/DCNT, DCNT and CNT catalysts in H-type cell tests.

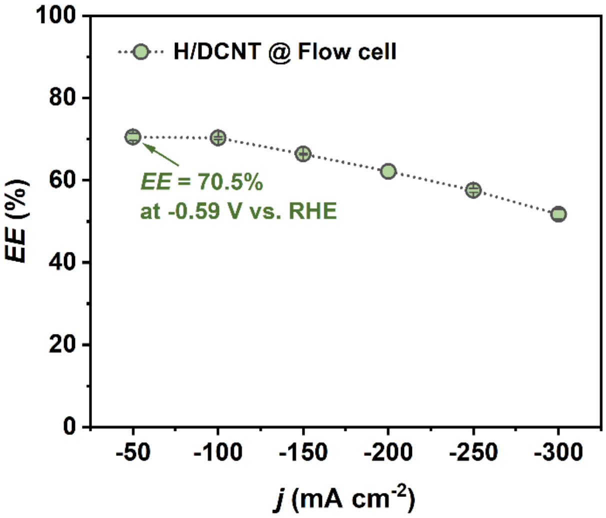

Figure S18. Energy efficiency (*EE*) over H/DCNT at different total current densities (*j*) in flow cell test.

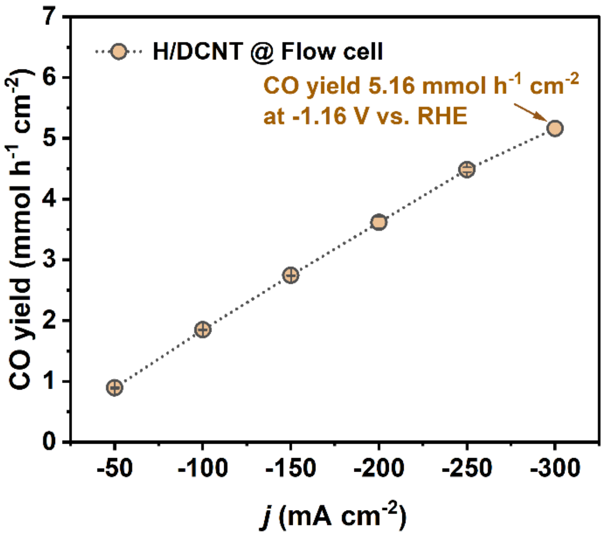

Figure S19. CO yield over H/DCNT at different total current densities (*j*) in flow cell test.

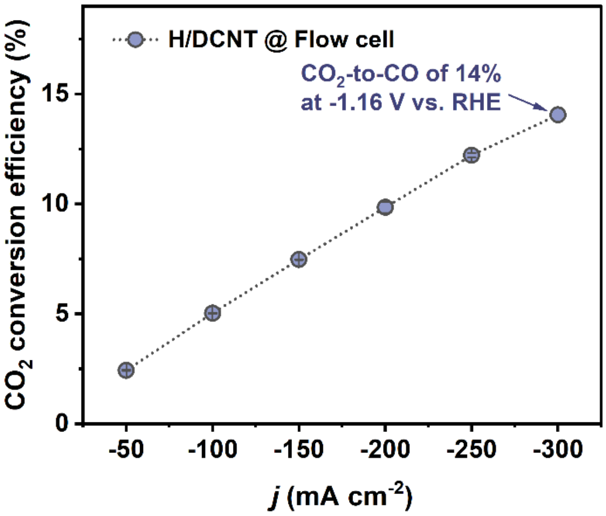

Figure S20. CO_2 conversion efficiency over H/DCNT at different total current densities (*j*) in flow cell test.

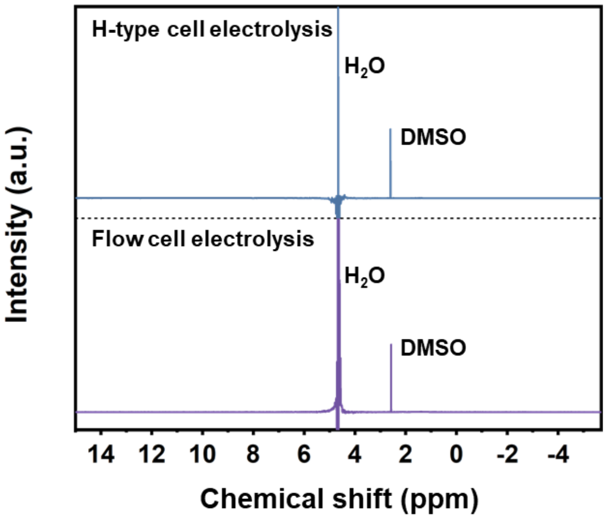

Figure S21. ^{1}H NMR spectra of the solution from H-type cell and flow cell after electrolysis.

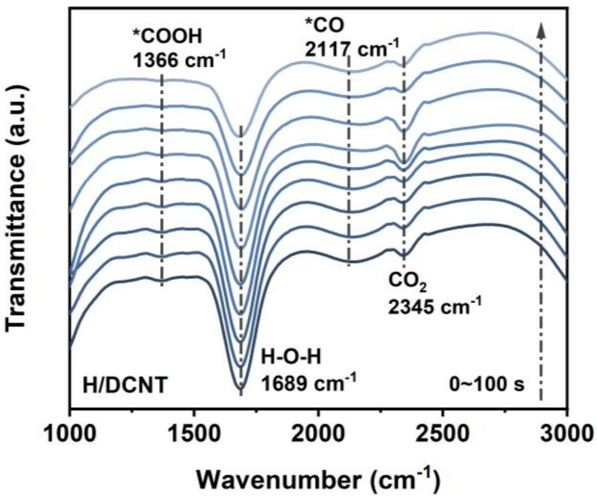

Figure S22. *In situ* FTIR spectra of H/DCNT.

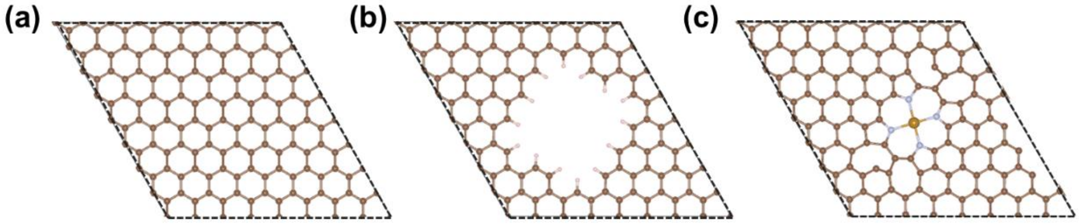

Figure S23. The structures of (a) CNT, (b) DCNT with the defect of type IV and (c) H/DCNT.

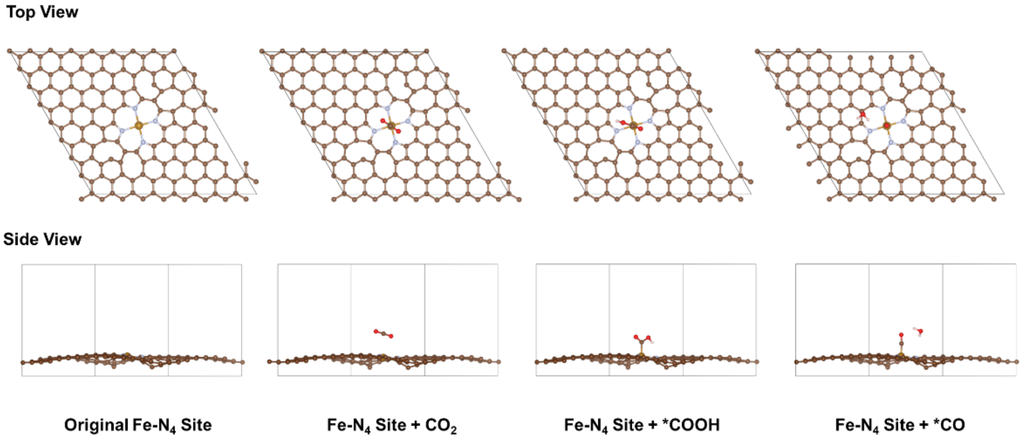

Figure S24. The optimized structures of H/DCNT and the intermediates at different steps for CO_2-to-CO conversion process.

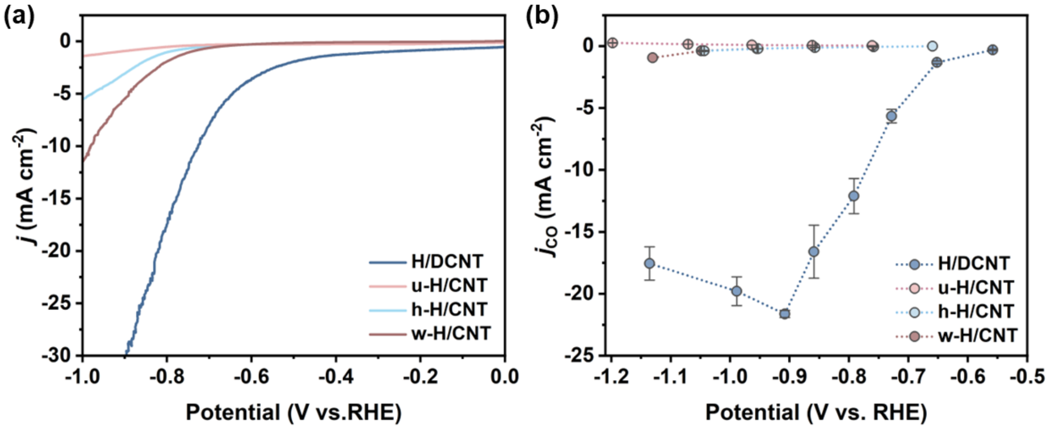

Figure S25. (a) Linear sweep voltammetry (LSV) curves and (b) partial current density for CO (j_{CO}) over the contrast catalysts of H/DCNT, u-H/CNT, h-H/CNT and w-H/CNT, respectively.

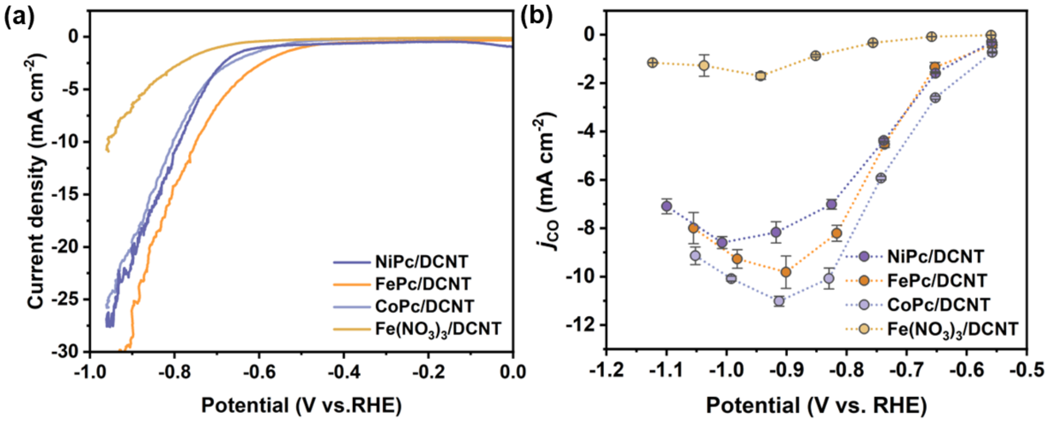

Figure S26. (a) Linear sweep voltammetry (LSV) curves and (b) partial current density for CO (j_{CO}) of NiPc/DCNT, FePc/DCNT, CoPc/DCNT and Fe(NO$_3$)$_3$/DCNT catalysts.

Table S1. The comparison of the energy consumption for preparation of L-H-CNT, π-H-CNT, and H/DCNT.

Methodology	**Catalyst**	**Process**	**Machine Power [a] (Watt)**	**Operation Time (h)**	**Electricity Consumption (kW h)**
Ligand-assisted limitation	L-H-CNT	Ultrasonication	360	2+0.92 [b]	98.5
		Stirring (@4 °C)	2600	25	
		Dry	1400	6+12 [b]	
		Stirring (@80 °C)	260	24	
π-π stacking interaction	π-H-CNT	Stirring (@RT)	30	12	17.2
		Dry	1400	12	
Defect-mediated integration	H/DCNT	Ultrasonication	360	0.5	0.4
		Microwave	1200	0.17	

Note:

[a] These data are derived from the power indicated on the nameplate of the equipment used in the laboratory.

[b] The operating time is divided into two parts, the first part corresponds to the energy consumption generated for synthesis of aminated CNT and the other part is the energy consumption for chemical grafting process, as mentioned in the section of 'Synthesis of L-H-CNT and π-H-CNT' in the Supporting Information.

Table S2. Composition and the corresponding mass ratio in Hemin.

Species	**Chemical Formula**	**Molecular Weight**	**Weight Ratio**
Hemin	$C_{34}H_{32}ClN_4O_4Fe$	651.96 g mol^{-1}	100%
Methyl	$-CH_3$	15*4=60 g mol^{-1}	9.2%
Vinyl	$-CH=CH_2$	27*2=54 g mol^{-1}	8.3%
Propionyloxy	$-CH_2CH_2COOH$	73*2=146 g mol^{-1}	22.4%
Chlorine	$-Cl$	35.5*1=35.5 g mol^{-1}	5.4%
Fe-macrocycle	$C_{20}H_4N_4Fe$	356.46 g mol^{-1}	54.7%

Table S3. EXAFS fitting parameters at the Fe K-edge for various samples (S_0^2=0.752).

Sample	**Shell**	***CN***^{a}	***R***(Å)^b	**σ^2(Å^2)**^{c}	**Δ*E*$_0$(eV)**^{d}	***R* factor**
Fe foil	Fe-Fe	8*	2.48±0.01	0.0050±0.0014	7.7±2.5	0.0075
	Fe-Fe	6*	2.86±0.01	0.0071±0.0029		
FePc	Fe-N	4.0±0.1	1.99±0.02	0.0092±0.0024	6.2±2.4	0.0085
	Fe-C	8.0±0.4	2.93±0.02	0.0062±0.0024		
H/DCNT	Fe-N	4.4±0.7	1.96±0.01	0.0055±0.0038	3.4±0.8	0.0104
	Fe-Fe	1.5±0.7	3.09±0.02	0.0202±0.0092	6.6±1.2	

^{a}*CN*, coordination number; ^{b}*R*, distance between absorber and backscatter atoms; $^c\sigma^2$, Debye-Waller factor to account for both thermal and structural disorders; $^d\Delta E_0$, inner potential correction; *R* factor, the goodness of the fit.

Table S4. Activity comparison of H/DCNT with recently reported representative advanced catalysts.

Label	Catalysts	Electrolyte	Potential (V vs. RHE)	*FE*$_{CO}$ (%)	*j* (mA cm^{-2})	TOF (h^{-1})	Metal content (wt%)	Device	Reference
a	NiSA-N-CNTs	0.5 M $KHCO_3$	−0.55	89	~ −14	42,120	~20 (XANES)	H-type cell	[8]
b	COF-367-Co	0.5 M $KHCO_3$	−0.65	90	/	9,400	/	H-type cell	[9]
c	Ni-NCB	0.5 M $KHCO_3$	−0.66	>95	~ −8	34,776	0.27 (ICP)	H-type cell	[10]
d	Ni-N-MEGO	0.5 M $KHCO_3$	−0.69	>90	~ −26.8	864	8.3 (ICP)	H-type cell	[11]
e	A-Ni-NSG	0.5 M $KHCO_3$	−0.72	97	~ −22	14,800	2.8 (ICP)	H-type cell	[12]
f	ZnNx/C	0.5 M $KHCO_3$	−0.73	~60	−13.62	9,969	0.1 (ICP)	H-type cell	[13]
g	Ni_1-1N-C	0.5 M $KHCO_3$	−0.8	97	−27.8	11,315	1.75 (ICP)	H-type cell	[14]
h	N_3NiPc-CNT	0.5 M $KHCO_3$	−0.93	100	~ −40	32,338	0.43 (ICP)	H-type cell	[15]
i	PyNiPc	0.5 M $KHCO_3$	−0.93	~100	~ −30	13,000	0.50 (ICP)	H-type cell	[16]
j	Zn-based MOFs	1 M KOH	−0.97	~94	−34.9	1,361	/	Flow cell	[17]
k	Ni-N-C	1 M KOH	−1.00	~80	−1000	274,000	1.10 (ICP)	Flow cell	[18]
l	Ni@CC-T	0.5 M $KHCO_3$	−1.00	~100	~ −23	22,489	0.32 (XPS)	H-type cell	[19]
m	Ca-N_3O SAC	0.5 M $KHCO_3$	−1.05	≥90	−27	15,000	0.67 (/)	H-type cell	[20]
n	NC-CNTs(Ni)	0.1 M $KHCO_3$	−0.89	~85	−10	11,650	0.087 (ICP)	H-type cell	[21]
o	Ni@C_3N_4-CN	0.1 M $KHCO_3$	−1.178	≥90	~ −47	22,000	1.08 (ICP)	H-type cell	[22]
/	**H/DCNT**	**0.1 M $KHCO_3$**	**−0.91**	**80.5**	**−27**	**76,000**	**0.24 (ICP)**	**H-type cell**	**This work**
/	**H/DCNT**	**1 M $KHCO_3$**	**−1.16**	**92.2**	**−300**	**241,000**	**0.24 (ICP)**	**Flow cell**	**This work**

Table S5. The comparison of performance for CO_2-to-CO conversion over the advanced catalysts in MEA test, while the anode reaction is oxygen evolution reaction.

Catalysts	**Cell Voltage (V)**	**Total Current (A)**	***FE*$_{CO}$ (%)**	**Reference**
Ni-N/NCNT	2.4	~1.2	~70	23
	2.1	~0.5	96.7	
Ni@NCH-1000	3	0.4	>95	24
	2.4	~0.2	>95	
Ni-GS-1000	2.6	~1.4	>93	25
	3	1.9	99	
NiN_x/NCNT	2.13	0.1	99	26
	2.62	0.3	99	
Ag/GDL	~3.5	0.05	96	27
	~4.3	0.1	>90	
Ni-SA-NCs	3	0.38	99	28
	2.6	0.14	~99	
H/DCNT	**2.7**	**1**	**96.5**	**This work**
	3.4	**5**	**97.5**	

Reference

1. C.-X. Zhao, J.-N. Liu, J. Wang, C. Wang, X. Guo, X.-Y. Li, X. Chen, L. Song, B.-Q. Li and Q. Zhang, *Sci. Adv.*, 2022, **8**, eabn5091.
2. P. E. Blöchl, *Phys. Rev. B*, 1994, **50**, 17953-17979.
3. G. Kresse and J. Hafner, *J. Non-Cryst. Solids*, 1993, **156-158**, 956-960.
4. G. Kresse and J. Hafner, *Phys. Rev. B*, 1994, **49**, 14251-14269.
5. J. P. Perdew, K. Burke and M. Ernzerhof, *Phys. Rev. Lett.*, 1996, **77**, 3865-3868.
6. M. Methfessel and A. T. Paxton, *Phys. Rev. B*, 1989, **40**, 3616-3621.
7. K. Mathew, R. Sundararaman, K. Letchworth-Weaver, T. A. Arias and R. G. Hennig, *J. Chem. Phys.*, 2014, **140**, 084106
8. Y. Cheng, S. Zhao, B. Johannessen, J. P. Veder, M. Saunders, M. R. Rowles, M. Cheng, C. Liu, M. F. Chisholm, R. De Marco, H. M. Cheng, S. Z. Yang and S. P. Jiang, *Adv. Mater.*, 2018, **30**, 1706287.
9. S. Lin, C. S. Diercks, Y.-B. Zhang, N. Kornienko, E. M. Nichols, Y. Zhao, A. R. Paris, D. Kim, P. Yang, O. M. Yaghi and C. J. Chang, *Science*, 2015, **349**, 1208-1213.
10. T. Zheng, K. Jiang, N. Ta, Y. Hu, J. Zeng, J. Liu and H. Wang, *Joule*, 2019, **3**, 265-278.
11. Y. Cheng, S. Zhao, H. Li, S. He, J.-P. Veder, B. Johannessen, J. Xiao, S. Lu, J. Pan, M. F. Chisholm, S.-Z. Yang, C. Liu, J. G. Chen and S. P. Jiang, *Appl. Catal. B-Environ.*, 2019, **243**, 294-303.
12. H. Yang, S. Hung, S. Liu, K. Yuan, S. Miao, L. Zhang, X. Huang, H. Wang, W. Cai, R. Chen, J. Gao, X. Yang, W. Chen, Y. Huang, H. Chen, C. M. Li, T. Zhang and B. Liu, *Nat. Energy*, 2018, **3**, 140-147.
13. F. Yang, P. Song, X. Liu, B. Mei, W. Xing, Z. Jiang, L. Gu and W. Xu, *Angew. Chem. Int. Ed.*, 2018, **57**, 12303-12307.
14. L. Jiao, W. Yang, G. Wan, R. Zhang, X. Zheng, H. Zhou, S. H. Yu and H. L. Jiang, *Angew. Chem. Int. Ed.*, 2020, **59**, 20589-20595.
15. D.-D. Ma, S.-G. Han, C. Cao, W. Wei, X. Li, B. Chen, X.-T. Wu and Q.-L. Zhu, *Energy Environ. Sci.*, 2021, **14**, 1544-1552.
16. D. Ma, S. Han, C. Cao, X. Li, X. Wu and Q. Zhu, *Appl. Catal. B-Environ.*, 2020, **264**, 118530.
17. T. A. Al-Attas, N. N. Marei, X. Yong, N. G. Yasri, V. Thangadurai, G. Shimizu, S. Siahrostami and M. G. Kibria, *ACS Catal.*, 2021, **11**, 7350-7357.
18. Y. Zhou, Q. Zhou, H. Liu, W. Xu, Z. Wang, S. Qiao, H. Ding, D. Chen, J. Zhu, Z. Qi, X. Wu, Q. He and L. Song, *Nat Commun*, 2023, **14**, 3776.
19. T. Wang, J. Wang, C. Lu, K. Jiang, S. Yang, Z. Ren, J. Zhang, X. Liu, L. Chen, X. Zhuang and J. Fu, *Adv. Mater.*, 2023, **35**, e2205553.
20. Q. Wang, M. Dai, H. Li, Y. R. Lu, T. S. Chan, C. Ma, K. Liu, J. Fu, W. Liao, S. Chen, E. Pensa, Y. Wang, S. Zhang, Y. Sun, E. Cortes and M. Liu, *Adv. Mater.*, 2023, **35**, e2300695.
21. Q. Fan, P. Hou, C. Choi, T. S. Wu, S. Hong, F. Li, Y. L. Soo, P. Kang, Y. Jung and Z. Sun, *Adv. Energy Mater.*, 2019, **10**, 1903068.
22. Q. Wang, K. Liu, K. Hu, C. Cai, H. Li, H. Li, M. Herran, Y. R. Lu, T. S. Chan, C. Ma, J. Fu, S. Zhang, Y. Liang, E. Cortes and M. Liu, *Nat Commun*, 2022, **13**, 6082.
23. Y. E. Kim, Y. N. Ko, B.-S. An, J. Hong, Y. E. Jeon, H. J. Kim, S. Lee, J. Lee and W. Lee, *ACS Energy Lett.*, 2023, **8**, 3288-3296.
24. R. Daiyan, X. Zhu, Z. Tong, L. Gong, A. Razmjou, R.-S. Liu, Z. Xia, X. Lu, L. Dai and R. Amal, *Nano Energy*, 2020, **78**, 105213.
25. J. Leverett, J. A. Yuwono, P. Kumar, T. Tran-Phu, J. Qu, J. Cairney, X. Wang, A. N. Simonov, R. K. Hocking, B. Johannessen, L. Dai, R. Daiyan and R. Amal, *ACS Energy Lett.*, 2022, **7**, 920-928.

26. R. Zhao, Y. Wang, G. Ji, J. Zhong, F. Zhang, M. Chen, S. Tong, P. Wang, Z. Wu, B. Han and Z. Liu, *Adv. Mater.*, 2023, **35**, e2205262.
27. X. Wang, P. Li, J. Tam, J. Y. Howe, C. P. O'Brien, A. Sedighian Rasouli, R. K. Miao, Y. Liu, A. Ozden, K. Xie, J. Wu, D. Sinton and E. H. Sargent, *Nat. Sustain.*, 2024, **7**, 931-937.
28. H.-Y. Jeong, M. Balamurugan, V. S. K. Choutipalli, E.-s. Jeong, V. Subramanian, U. Sim and K. T. Nam, *J. Mater. Chem. A*, 2019, **7**, 10651-10661.